17th World Conference on Earthquake Engineering, 17WCEE
Sendai, Japan – September 13th to 18th 2020

EVALUATION OF LATERAL FORCE ON A SQUARE CYLINDER FIXED IN CHANNEL FLOW USING NON-HYDROSTATIC SWE EQUATIONS

T. Koyama(1)

(1) *Assistant Professor, the University of Tokyo, koyama@arch.t.u-tokyo.ac.jp*

Abstract

The evaluation of lateral forces acting on structures due to quasi-steady tsunami flows is crucial in the design of buildings able to withstand tsunami forces. Though formulas have been developed to evaluate this force, most have been developed under the assumption that the building is freestanding without any surrounding objects. In reality, the surrounding objects change the nature of the flow and thus the force acting on the structure. In this research, non-hydrostatic shallow water equations(NSWE) are developed and its applicability in evaluating the effect of surrounding objects constraining the flow is investigated via numerical simulations. The NSWE are derived from the Navier-Stokes and continuity equations through a Galerkin method in which the in-plane and depth directional velocities are assumed to have a linear distribution and the non-hydrostatic pressure a quadratic distribution in the depth direction. The derived NSWE are implemented in the open source software OpenFOAM[5]. The proposed NSWE is shown to have superior dispersion characteristics compared to the hydrostatic shallow water equations with Boussinesq assumption. The effectiveness of the NSWE is confirmed through evaluation of the drag coefficient of a square cylinder fixed in open channel flow and comparison with the experimental results by Qi et al[6]. It is shown that the addition of the non-hydrostatic pressure components greatly improves the flow characteristics behind the square cylinder resulting in closer matching of the simulation with the experiments.

Keywords: tsunami, shallow water equation, non-hydrostatic pressure, open channel flow, OpenFOAM

1. Introduction

The evaluation of lateral forces acting on structures due to quasi-steady tsunami flows is crucial in the design of buildings able to withstand tsunami forces. Though formulas have been developed to evaluate this force, most have been developed under the assumption that the building is freestanding without any surrounding objects. In reality, the surrounding objects change the nature of the flow and thus the force acting on the structure.

The effect of the surrounding objects constraining the flow on the lateral force applied to structures can be investigated through small-scale model hydraulic experiments, but restrictions on the experimental facilites prohibit experimentation with various setups as well as sizes. On the other hand numerical simulation do not have such physical restrictions and are limited only by the computational resources and numerical methods at hand. A numerical simulation of the free surface flow acting on the structure employing the full 3D Navier-Stokes equation results in fine detail of the pressure acting on the structure as well as the integral lateral force, but can be computationally costly. The use of the 2D standard shallow water equations, which are a depth integrated version of the Navier-Stokes equation, is an alternative method with less degrees of freedom requiring less computational effort[1]. Its shortcoming in evaluating the lateral forces on structures arises from the assumption of hydrostatic pressure, which may not always be valid in complex flows around structures. Non-hydrostatic extensions of the shallow water equations employing Boussinesq terms have been developed and employed in tsunami simulations, but their emphasis is in improving the dispersive characteristics of the governing equations.

In this research, a NSWE applicable to the evaluation of lateral forces is presented based on the VAM by Ghamry and Steffler[2], which take into account linear and quadratic non-hydrostatic pressure distributions as well as linear velocity distributions. Though the equations are similar, the equations presented in this paper are developed through the Galerkin method, resulting in equations which are easier to understand and implement in a finite volume setting such as the OpenFOAM[5] software. The validity of the implementation is verified by checking its dispersion properties and comparing with previous hydraulic experiments. The dispersion character is shown to be superior compared to standard Boussinesq assumptions. Its applicability in evaluating the lateral force in constrained flows is verified through numerical simulations of a square cylinder fixed in open channel flow and compared to those of Qi et al.'s experiments[6]. The choking type of phenomena is properly displayed with similar variation of the drag coefficient with respect to the Froude number.

2. Non-hydrostatic shallow water equation

2.1 Derivation

The following Navier-Stokes equation and continuity equation with incompressibility is assumed to govern the behavior of the water.

$$\frac{\partial \mathbf{u}}{\partial t} + \nabla \cdot \mathbf{u} \otimes \mathbf{u} + \nabla p - \nabla \cdot \boldsymbol{\tau}^T - g\mathbf{e}_3 = \mathbf{0}, \tag{1}$$

$$\nabla \cdot \mathbf{u} = 0, \tag{2}$$

The setup is shown in Fig.1, where x_i denotes the Cartesian coordinates with x_3 in the depth direction and t the time. $\mathbf{u}(:= [u, v, w])$ is the velocity vector, p the pressure scaled by the fluid density ρ(=1000[kg/m^3]), $\boldsymbol{\tau}$ the deviatoric stresses scaled by ρ, and g(=9.81[m/s^2]) is the gravitational constant. The surface of the bottom floor is defined by z_b, the surface of the water by z_s, the water depth $z_s - z_b$ by the symbol h.

The Galerkin method is employed to derive the non-hydrostatic shallow water equation, where the velocity and pressure are assumed to have the following interpolated form,

$$\mathbf{u}(\mathbf{x}) = [N_0(\alpha), N_1(\alpha)] \begin{bmatrix} \mathbf{u}_0(x_1, x_2) \\ \mathbf{u}_1(x_1, x_2) \end{bmatrix}, \tag{3}$$

$$p(\mathbf{x}) = [Q_0(\alpha), Q_1(\alpha), Q_2(\alpha)] \begin{bmatrix} p_0(x_1, x_2) \\ p_1(x_1, x_2) + gh \\ p_2(x_1, x_2) \end{bmatrix}, \tag{4}$$

$$\alpha(\mathbf{x}) = \frac{x_3 - z_b(x_1, x_2)}{z_s(x_1, x_2) - z_b(x_1, x_2)}. \tag{5}$$

Here N_0, N_1 are the shape functions for the velocity distribution in the x_3 direction, and Q_0, Q_1, Q_2 are shape functions for the pressure distribution in the x_3 direction. The shape functions are defined in terms of α, a non-dimensional parameter denoting the location within the depth, which takes a value of 0 at the bottom floor and 1 at the water surface. The form of these functions are shown in Fig.2. N_0, N_1 are the 0th and 1st order Legendre polynomials defined on the interval $[0, 1]$ and are able to represent the constant and linear velocity profiles. $Q_0 = N_0$ and Q_1 and Q_2 are 1st and 2nd order polynomials defined to take a value of 0 at the water surface ($\alpha = 1$) and normalized to a magnitude of 1 at the bottom floor($\alpha = 0$), and are orthogonal to each other in the $L^2_{[0,1]}$ norm. Q_1 represents a linear variation in the non-hydrostatic pressure and Q_2 represents a quadratic variation. $\mathbf{u}_0$,$\mathbf{u}_1$ are the constant and linear contributions to the velocity and p_0,p_1,p_2 are the constant, linear, and quadratic contributions to the non-hydrostatic pressure, and only depend on the in-plane coordinates x_1, x_2.

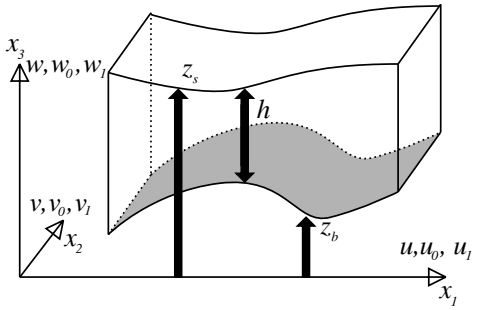

Fig. 1 Configuration of the problem

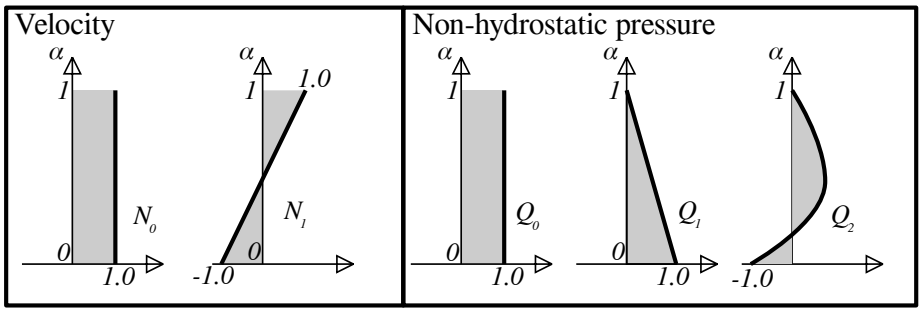

Fig. 2 Shape functions

The Galerkin method applied to the Navier-Stokes equation and continuity equation with the test functions $\delta\mathbf{u}$, δp, on the interval $[z_b, z_s]$ result in the following equations.

$$\int_{z_b}^{z_s} \delta\mathbf{u} \cdot \left(\frac{\partial \mathbf{u}}{\partial t} + \nabla \cdot \mathbf{u} \otimes \mathbf{u} + \nabla p - \nabla \cdot \boldsymbol{\tau}^T - g\mathbf{e}_3 \right) dx_3 = 0, \tag{6}$$

$$\int_{z_b}^{z_s} \delta p \left(\nabla \cdot \mathbf{u} \right) dx_3 = 0. \tag{7}$$

Combining these with the following kinematic boundary condition at the surface and bottom floor, which relate the vertical velocity w with the in-plane velocities u, v,

$$w(x,y,z_b) - u(x,y,z_b)\frac{\partial z_b}{\partial x_1} - v(x,y,z_b)\frac{\partial z_b}{\partial x_2} = 0, \tag{8}$$

$$w(x,y,z_s) - u(x,y,z_s)\frac{\partial z_s}{\partial x_1} - v(x,y,z_s)\frac{\partial z_s}{\partial x_2} = 0, \tag{9}$$

result in the following NSWE.

$$\begin{aligned} \frac{\partial}{\partial t}\left(h\mathbf{u}_0\right) + \nabla \cdot \left\{ \mathbf{u}_0 \otimes h\mathbf{u}_0 + \frac{1}{3}\mathbf{u}_1 \otimes h\mathbf{u}_1 \right\} \quad &+ \quad gh\,\nabla\left\{h + z_b\right\}, \\ +\nabla\left\{ \frac{1}{2}hp_1 + \frac{1}{6}hp_2 \right\} + h\nabla p_0 \quad &+ \quad (p_1 - p_2)\nabla z_b - \nabla \cdot (h\boldsymbol{\tau}_{00}) + \boldsymbol{\tau}_b = \mathbf{0} \end{aligned} \tag{10}$$

$$\begin{aligned} \frac{\partial}{\partial t}\left(hw_0\right) + \nabla \cdot \left\{ \mathbf{u}_0 hw_0 + \frac{1}{3}\mathbf{u}_1 hw_1 \right\} & \\ - \quad (p_1 - p_2) - \nabla \cdot (h\boldsymbol{\tau}_{0z}) - \boldsymbol{\tau}_b \cdot \nabla z_b = 0, \end{aligned} \tag{11}$$

$$\begin{aligned}
&\frac{\partial}{\partial t}\left(h\mathbf{u}_1\right)+\nabla\cdot\left\{\mathbf{u}_0\otimes h\mathbf{u}_1+\mathbf{u}_1\otimes h\mathbf{u}_0\right\}-\mathbf{u}_0\nabla\cdot\left(h\mathbf{u}_1\right)\\
&\qquad+\nabla\left\{-\frac{1}{2}hp_1+\frac{1}{2}hp_2\right\}+p_1\nabla h+p_2\nabla(h+4z_b)\\
&-\nabla\cdot\left(h\boldsymbol{\tau}_{11}\right)-\left\{3\boldsymbol{\tau}_{00}\cdot\nabla(h+2z_b)+\boldsymbol{\tau}_{11}\cdot\nabla h-6\boldsymbol{\tau}_{0z}\right\}-3\boldsymbol{\tau}_b \;=\; \mathbf{0} \qquad (12)\\
&\frac{\partial}{\partial t}\left(hw_1\right)+\nabla\cdot\left\{\mathbf{u}_0hw_1+\mathbf{u}_1hw_0\right\}-w_0\nabla\cdot\left(h\mathbf{u}_1\right)-4p_2\\
&-\nabla\cdot\left(h\boldsymbol{\tau}_z^1\right)-\left\{3\boldsymbol{\tau}_{0z}\cdot\nabla(h+2z_b)+\boldsymbol{\tau}_{1z}\cdot\nabla h-6\tau_{zz}^0\right\}+3\boldsymbol{\tau}_b\cdot\nabla z_b \;=\; 0 \qquad (13)
\end{aligned}$$

$$\begin{aligned}
\frac{\partial h}{\partial t}+\mathrm{div}\left(h\mathbf{u}_0\right) &= 0 \qquad (14)\\
-\frac{1}{2}h\mathrm{div}\left(\mathbf{u}_0\right)+\frac{1}{3}\mathrm{div}\left(h\mathbf{u}_1\right)-\frac{1}{6}h\mathrm{div}(\mathbf{u}_1)+\frac{\partial z_b}{\partial t}+\mathbf{u}_0\cdot\nabla z_b &= w_0 \qquad (15)\\
-\frac{1}{6}h\mathrm{div}\left(\mathbf{u}_0\right)+\frac{1}{3}\mathrm{div}\left(h\mathbf{u}_1\right)-\frac{1}{2}h\mathrm{div}(\mathbf{u}_1)+\left(\frac{4}{3}\mathbf{u}_1-\mathbf{u}_0\right)\cdot\nabla z_b-\frac{\partial z_b}{\partial t} &= \frac{4}{3}w_1-w_0 \qquad (16)
\end{aligned}$$

In these equations, $\nabla := [\frac{\partial}{\partial x_1}, \frac{\partial}{\partial x_2}]$ denotes the operator acting only on the two in-plane dimensions x_1, x_2 and $\mathbf{u}_0 := [u_0, v_0]$, $\mathbf{u}_1 := [u_1, v_1]$. $\boldsymbol{\tau}_{00}$, $\boldsymbol{\tau}_{11}$,$\boldsymbol{\tau}_{0z}$, $\boldsymbol{\tau}_{1z}$, τ_{0zz},τ_{1zz} are the deviatoric stresses and $\boldsymbol{\tau}_b$ is the shear stress at the bottom floor, whose definitions will be given later in the section. The constant pressure p_0 corresponds to the pressure boundary condition at the water surface. In the current implementation, the surface tension is modeled as the curvature of the surface resulting in,

$$p_0 \;=\; \frac{\kappa}{\rho}\nabla^2 h\,, \qquad (17)$$

where κ is the surface tension of water (=70[mN/m]).

The proposed NSWE consist of 9 equations in 9 unknowns, which are the 4 in-plane velocities $\mathbf{u}_0$, $\mathbf{u}_1$, the 2 out-of-plane velocities w_0, w_1, the water depth h, and the 2 non-hydrostatic pressure terms p_1, p_2. The equations presented here differ from those by Ghamry[2] in several aspects. First of all, the governing equations by Ghamry are not strictly derived from a Galerkin method and an approximation of the point-wise constraints Eq.(8),(9) is employed. This introduces an additional equation allowing one to introduce a quadratic interpolation into the vertical velocity w, resulting in one additional equation and unknown for a total of 10 equations in 10 unknowns. The proposed method utilizes the constraint equations Eq.(15),(16) derived from the Galerkin method applied to the continuity equation. Second, the interpolation functions for the vertical velocity w are chosen the same as the in-plane velocities, resulting in a symmetric representation of the governing equations, easier implementation, as well as retaining the orthogonality of the interpolation functions in the $L^2_{[0,1]}$ norm. Third, the present implementation assumes orthogonal polynomials for the non-hydrostatic pressure terms resulting in better numerical conditioning. Fourth, the equations are organized so that their structure is clearer to understand.

By proper reduction, Eqs.(10)-(16) revert to the standard hydrostatic shallow water equation or shallow water equation with Boussinesq term. The possible cases are shown in Table1. The full equations correspond to case "2 term". The case "1 term" corresponds to the case where a linear non-hydrostatic pressure distribution is assumed. All terms related to p_2 are assumed to be zero and only Eqs. (10),(11),(14),(15) are treated. If one assumes the coefficient of $\nabla h p_1$ in Eq. (10) to be $2/3$ instead of $1/2$, one obtains a formulation with a dispersion relationship equivalent to the Boussinesq assumption[3] corresponding to case "Boussinesq". Further assuming $p_1 = 0$, the equations reduce to the hydrostatic shallow water equation with equations (10) and (14).

Table 1 Considered cases

Case	Assumption	Description
Hydrostatic	$q_1 = q_2 = 0$	Hydrostatic SWE
1 term	$q_2 = 0$	NSWE with linear pressure distribution
2 term	-	NSWE with combined linear and quadratic pressure distribution
Boussinesq	$q_2 = 0$, $\nabla\frac{2}{3}hp_1$ in Eq.(10)	Nonhydrostatic SWE with Boussinesq term

The shear stress at the floor bottom $\boldsymbol{\tau}_b$ is evaluated using Manning formula where,

$$\alpha = g\frac{n^2}{h^{1/3}}\frac{|h\mathbf{u}_0 - h\mathbf{u}_1|}{h^2}\,, \tag{18}$$

$$\boldsymbol{\tau}_b = \alpha|h\mathbf{u}_0 - h\mathbf{u}_1|\,. \tag{19}$$

Here, n is the Manning coefficient. The deviatoric stress $\boldsymbol{\tau}$, is also decomposed into its constant and linear contribution as,

$$\boldsymbol{\tau} = [N_0, N_1]\begin{bmatrix}\boldsymbol{\tau}_0\\ \boldsymbol{\tau}_1\end{bmatrix} \quad ,\boldsymbol{\tau}_0 = \begin{bmatrix}\boldsymbol{\tau}_{00} & \boldsymbol{\tau}_{0z}\\ \boldsymbol{\tau}_{0z}^T & \tau_{0zz}\end{bmatrix} \quad ,\boldsymbol{\tau}_1 = \begin{bmatrix}\boldsymbol{\tau}_{11} & \boldsymbol{\tau}_{1z}\\ \boldsymbol{\tau}_{1z}^T & \tau_{1zz}\end{bmatrix}\,. \tag{20}$$

The $\boldsymbol{\tau}_{00}$, $\boldsymbol{\tau}_{11}$ are the in-plane deviatoric stresses. The deviatoric strain rate $\mathbf{D}$ is computed from the standard linear definition as,

$$\mathbf{D} = \frac{1}{2}\left[\nabla\mathbf{u} + \nabla\mathbf{u}^T\right] - \frac{1}{3}\nabla\cdot\mathbf{u} = [N_0, N_1]\begin{bmatrix}\mathbf{D}_0\\ \mathbf{D}_1\end{bmatrix}\,. \tag{21}$$

$$D_{0\alpha\beta} = \text{symm}\left\{\nabla\mathbf{u}_0\right\} - \frac{1}{h}\text{symm}\left\{\mathbf{u}_1\otimes\nabla h\right\} - \frac{2}{h}\text{symm}\left\{\mathbf{u}_1\otimes\nabla z_b\right\} \tag{22}$$

$$D_{1\alpha\beta} = \text{symm}\left\{\nabla\mathbf{u}_1\right\} - \frac{1}{h}\text{symm}\left\{\mathbf{u}_1\otimes\nabla h\right\} \tag{23}$$

$$D_{0\alpha z} = \frac{1}{2}\left\{2\frac{\mathbf{u}_1}{h} + \nabla w_0 - \frac{w_1}{h}\nabla h - \frac{w_2}{h}\nabla h - 2\frac{w_1}{h}\nabla z_b\right\} \tag{24}$$

$$D_{1\alpha z} = \frac{1}{2}\left\{\nabla w_1 - \frac{w_1}{h}\nabla h - 3\frac{w_2}{h}\nabla h - 6\frac{w_1}{h}\nabla z_b\right\} \tag{25}$$

$$D_{2\alpha z} = \frac{1}{2}\left\{\frac{\partial w_2}{\partial x_\alpha} - 2\frac{w_2}{h}\frac{\partial h}{\partial x_\alpha}\right\} \tag{26}$$

$$D_{0zz} = 2\frac{w_1}{h} \tag{27}$$

$$D_{1zz} = 6\frac{w_2}{h} \tag{28}$$

An LES type of approach is taken to evaluate the contribution of the turbulent stress[4] where,

$$\boldsymbol{\tau} = 2(\nu + \nu_t)\mathbf{D} \tag{29}$$

$$\nu_t = (0.173\Delta)^2\sqrt{2\overline{\mathbf{D}:\mathbf{D}}} \tag{30}$$

$$\overline{\mathbf{D}:\mathbf{D}} = \int_{z_b}^{z_s}\mathbf{D}:\mathbf{D}dx_3 = \mathbf{D}_0:\mathbf{D}_0 + \frac{1}{3}\mathbf{D}_1:\mathbf{D}_1 \tag{31}$$

$$\Delta = (\Delta x\Delta y h)^{\frac{1}{3}} \tag{32}$$

2.2 Linear dispersion characteristics

The dispersion characteristics of the proposed NSWE is investigated in this section. As shown in Fig.3, A constant bottom floor $z_b = 0$ is assumed and the equations are linearized around a fixed depth h_0 so that $h = h_0 + \eta$ with $\eta << 1$. Further assumption of no change in the x_2 direction results in the following 1D linearized equations[3].

$$h_0\frac{\partial u_0}{\partial t} + gh_0\frac{\partial \eta}{\partial x_1} + \frac{1}{2}h_0\frac{\partial p_1}{\partial x_1} + \frac{1}{6}h_0\frac{\partial p_2}{\partial x_1} = 0 \tag{33}$$

$$h_0\frac{\partial w_0}{\partial t} - (p_1 - p_2) = 0 \tag{34}$$

$$h_0\frac{\partial u_1}{\partial t} - \frac{1}{2}h_0\frac{\partial p_1}{\partial x_1} + \frac{1}{2}h_0\frac{\partial p_2}{\partial x_1} = 0 \tag{35}$$

$$h_0\frac{\partial w_1}{\partial t} - 4p_2 = 0 \tag{36}$$

$$\frac{\partial \eta}{\partial t} + h_0\frac{\partial u_0}{\partial x_1} = 0 \tag{37}$$

$$-\frac{1}{2}h_0\frac{\partial u_0}{\partial x_1} + \frac{1}{6}h_0\frac{\partial u_1}{\partial x_1} = w_0 \tag{38}$$

$$-\frac{1}{6}h_0\frac{\partial u_0}{\partial x_1} - \frac{1}{6}h_0\frac{\partial u_1}{\partial x_1} = \frac{4}{3}w_1 - w_0 \tag{39}$$

This results in 7 equations in 7 unknowns $(\eta, u_0, u_1, w_0, w_1, p_1, p_2)$. Assuming harmonic motion for all unknowns, for example the change in water surface is assumed the form $\eta = \hat{\eta}\exp^{i(kx_1-\omega t)}$, dispersion analysis for "2 term" results in the following equation,

$$\frac{\omega^2}{c_0^2k^2} = \frac{1 + \frac{1}{12}(kh_0)^2}{1 + \frac{5}{12}(kh_0)^2 + \frac{1}{144}(kh_0)^4}\,. \tag{40}$$

Here ω is the oscillating frequency, k is the wave number, and $c_0(=\sqrt{gh_0})$ is the wave speed in the shallow water limit. The ratio $\omega^2/c_0^2k^2$ is a nondimensionalized wave speed and kh_0 is a nondimensionalized wave number. In the "1 term" case, the dispersion relationship is,

$$\frac{\omega^2}{c_0^2k^2} = \frac{1}{1 + \frac{1}{4}(kh_0)^2}\,, \tag{41}$$

and the dispersion relationship for the case "Boussinesq" is,

$$\frac{\omega^2}{c_0^2k^2} = \frac{1}{1 + \frac{1}{3}(kh_0)^2}\,. \tag{42}$$

These equations plotted against the exact solution $\frac{\omega^2}{c_0^2k^2} = \frac{\tanh(kh_0)}{kh_0}$ is shown in Fig.4. The proposed NSWE has superior dispersion characteristics matching the exact curve to almost a nondimensional wave number of 10. Though "Boussinesq" closely matches the exact curve asymptotically in the vicinity of $kh_0 \approx 0$, "1 term" with a linear non-hydrostatic distribution better matches the exact curve when kh_0 is larger than 2. In the evaluation of tsunamis with SWEs, the waves are long compared to the sea depth, $kh_0 << 1$, and thus the Boussinesq assumption is often used and is advantageous. On other hand, in the evaluation of lateral forces on structures, waves my be shorter and thus the Boussinesq assumption may not be as effective. These aspects are further investigated in the next section through evaluation of the lateral force of surface piercing cylinders.

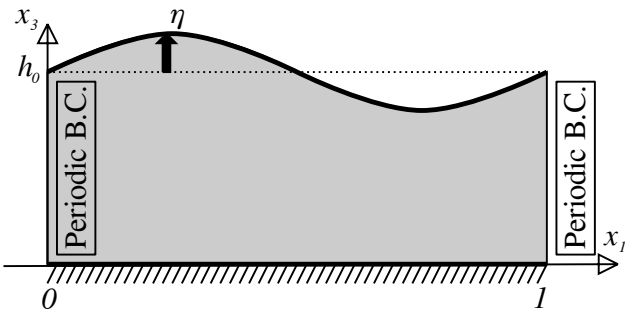

Fig. 3 Configuration used for dispersion analysis

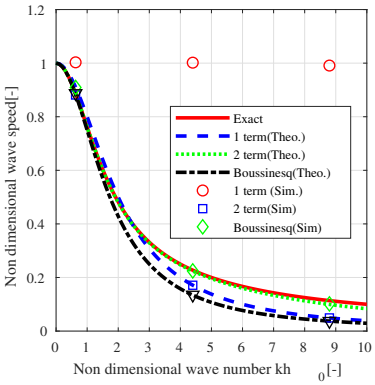

Fig. 4 Dispersion relationships

3. Numerical verification of the dispersion relationship

Here the non-hydrostatic shallow water equation implemented in the numerical software OpenFOAM[5] is validated by confirming the dispersion relationship in the small amplitude range.

The setup of the problem is shown in Fig.3[3]. A 1D domain in the x_1 direction with length L equal to 1[m] is assumed with periodic boundary conditions. An initial variation of the water surface in the form of a single sine wave is superimposed on a water depth of h_0. This sine wave is the analytical solution for the system of equation in Eq.(33) to (39). Under this applied initial displacement the surface vibrates freely and the vibration period T is measured. The non-dimensional wavelength is defined by $kh_0 = \frac{2\pi h_0}{L}$ and the non-dimensional wave speed squared is defined as $\frac{\omega^2}{c_0^2 k^2} = \frac{L^2}{gh_0T^2}$. The initial water depth h_0 is varied as $[0.1, 0.7, 1.4][m]$ and the magnitude of the initial water variation is given as 0.0001[m] to keep the wave variation small. The domain $[0, 1]$ is divided into 250 cells for sufficient wave resolution. Since the problem is simple and stability is not an issue, all terms in Eq.(10) to (16) are discretized using second order linear discretization. The effect of the bottom floor shear stress is not included in this simulation.

The dispersion relations for the 4 different cases shown in Table 1 are compared. The result obtained for the 3 different water depths h_0 is shown in Fig.4. As expected, the hydrostatic case has a constant wave speed irrespective of the wave number. The results from the 3 non-hydrostatic cases all lie perfectly on their assumed analytical curves from Eq.(40) to (41) validating the correctness of the implementation in its small wave regime.

4. Simulation of flow past a square cylinder

The applicability of the proposed NSWE to the evaluation of the lateral force of structures in open channels is investigated in this section. The setup is as shown in Fig.5 and based on the experiments conducted by Qi et al[6]. In the experiment by Qi, a square cylinder is set in an open channel 3[m] long and 0.5[m] wide and the lateral force is measured. The initial water depth in the absence of the cylinder and the channel volume flux are varied. Due to the presence of the square cylinder, the initial flow is disturbed upstream and downstream of the cylinder. The upstream and downstream depths are measured to compute the Froude number of the disturbed flow. When the blockage ratio, defined as the ratio of the width of the cylinder to the width of the channel, and Froude number of the initial flow is sufficiently large, choking may occur in which the upstream flow depth increases drastically.

In the simulation, the width of the square cylinder is set to 0.1[m] and the initial depth is set to 0.1[m]. 5 different channel volume fluxes varying from 0.013 to 0.065 [m^3/s^{-1}] (in increments of 0.013) are investigated

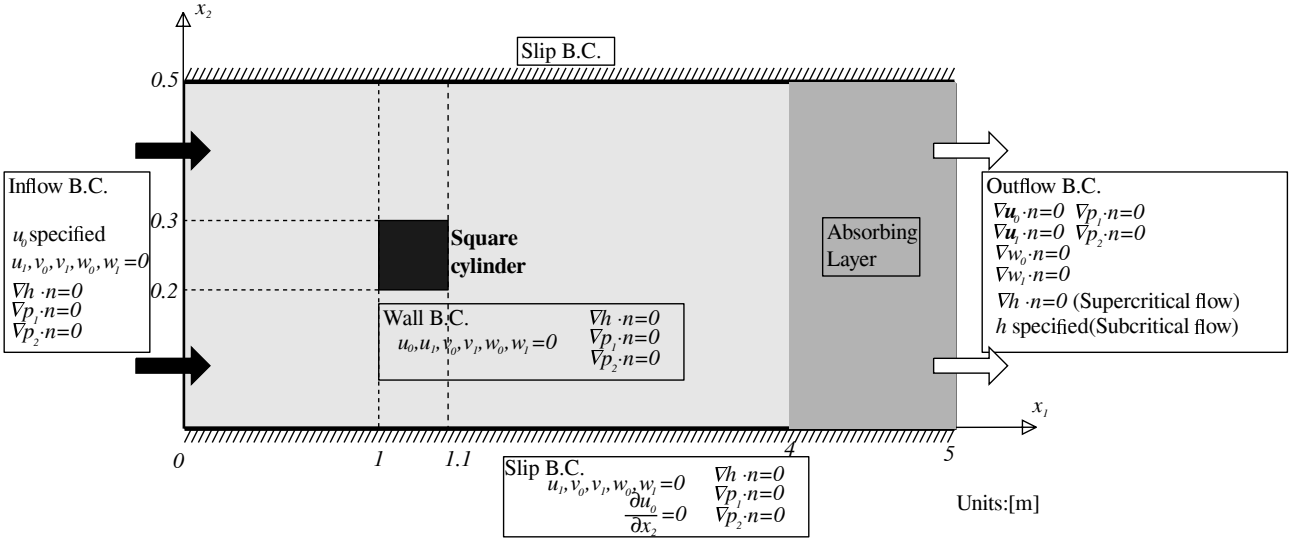

Fig. 5 Setup of the problem for a square cylinder in an open channel

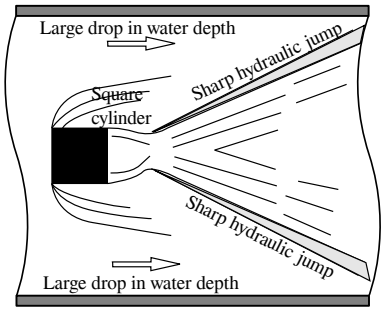

(a) Flow pattern observed in the experiment by Qi

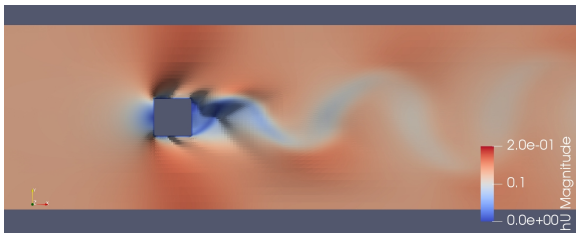

(b) Hydrostatic case

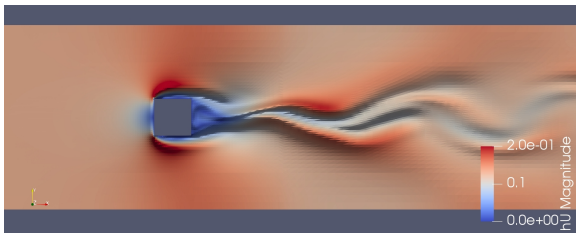

(c) 1 term nonhydrostatic case

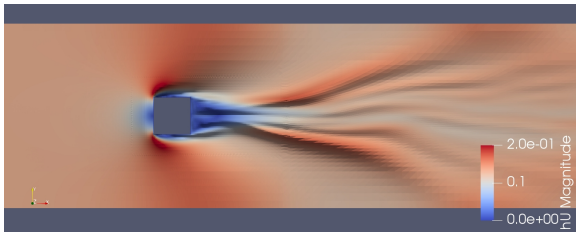

(d) 2 term nonhydrostatic case

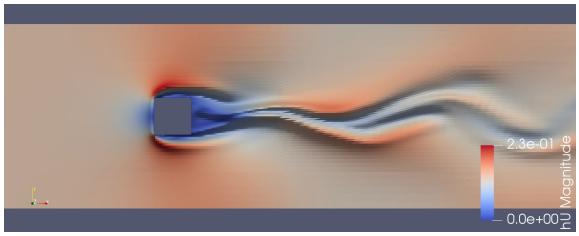

(e) Boussinesq nonhydrostatic case

Fig. 6 Flow patterns for choked flows

for the 4 different cases in Table 1. The size of the computational domain is set to 5[m], which is larger than the experiment, in order to minimized the effect of the downstream boundary conditions. The distance between the square cylinder and the inlet is not stated in the paper and set to 1[m]. The inflow and outflow treatment in the experiment is also not stated, and thus in this experiment the boundary conditions are set as stated in Fig.5. At the inflow boundary, the channel volume flux per width hu_0 is specified and a zero gradient is enforced on the water height. At the outflow, a zero gradient is enforced on the channel volume flux per width, and the average water height is specified in the case of subcritical flow, and a zero gradient is enforced in the case of supercritical flow. To minimize boundary reflections at the outflow boundary, a 1[m] long absorbing layer is set in front of the outflow boundary. At the open channel walls a slip boundary condition is employed and at the square cylinder a nonslip boundary condition is employed. The effect of the bottom floor shear stress is not included in this simulation.

In OpenFOAM, all time derivatives are discretized using the `Euler` method. The convective terms for the in-plane velocities $\mathbf{u}_0, \mathbf{u}_1$ are discretized using either a half and half mix of the `linearUpwind` and `linear` method or purely `linearUpwind` depending on the numerical convergence of the computation. The convective terms for the out of plane velocities w_0, w_1 are discretized using either the TVD monotonized central limiter or the TVD Sweby limiter($\beta = 2$). The time discretization is set so that the Courant number is kept below 0.125. The mesh is discretized so that near the cylinder the cell size is a 5[mm] square so that there are 20 cells across the width of the square. Away from the cylinder, the mesh is graded to 3 times this size.

Fig.6a shows a schematic of the flow for a channel volume flux of 0.065[m^3/s](hu_0=0.13[m^2/s]) (referencing the experiment by Qi[6]) in which choking occurs. Fig.6b to Fig.6e shows the corresponding simulated results. One observes that unlike the hydrostatic case, the 2 term non-hydrostatic case is able to reproduce the fanning hydraulic jump observed in the experiment. The 1 term and Boussinesq non-hydrostatic cases somewhat reproduce the fan but displays largely oscillating behavior compared to the experiment.

This difference in oscillating behavior can also be observed in the drag and lift coefficients(C_D and C_L) computed from the simulation. In this case, drag and lift coefficients are computed based on the disturbed upstream water height and velocity (following the approach by Qi[6]). The time histories of the drag and lift coefficients for choked and non-choked flows from Qi[6] are displayed in Fig.7a as a reference(the channel volume flux is not stated in Qi's paper). The simulated results for the 4 cases in Table 1 with volume flux of 0.065[m^3/s](hu_0=0.13[m^2/s],choked flow) and volume flux of 0.013[m^3/s](hu_0=0.026[m^2/s],nonchoked flow) are shown in Fig.7b-Fig.7e. One sees from the experimental values in Fig.7a that the drag coefficient of the choked flow is larger than the non-choked flow and that the lift coefficient is more oscillatory for non-choked flows compared to choked flows. The difference in drag coefficients between the choked and non-choked flows is more significant in the hydrostatic and 2 term non-hydrostatic case. The magnitude of the oscillatory behavior of the drag and the lift coefficients in the 2 term non-hydrostatic case seem to match the experimental results the closest.

In the case that the channel volume flux is increased from 0.013 to 0.065 [m^3/s^{-1}] with a fixed initial water height of 0.1[m], the initial upstream Froude number increases linearly but the increase in the disturbed upstream Froude number slows down due to choking. This phenomenon is also observed in the simulations. The relationship between the initial Froude number and disturbed upstream Froude number is shown in Fig.8 for the 4 cases along with the experimental value from Qi. As choking occurs, all simulated cases start to deviate from the straight line denoting equal initial and disturbed Froude number. However, the initial Froude number at which choking initiates and the value that the disturbed upstream Froude number converge to seem to differ. The hydrostatic case takes an almost constant value for initial Froude number larger than 0.8 as opposed to the other 3 cases in which the disturbed upstream Froude number continues to increase. The simulated results all seem to initiate choking at a larger initial upstream Froude number than the experiments. Among the 3 non-hydrostatic cases, the 2 term case yields the disturbed upstream Froude number closest to the experimental results, though there is noticeable difference between the values.

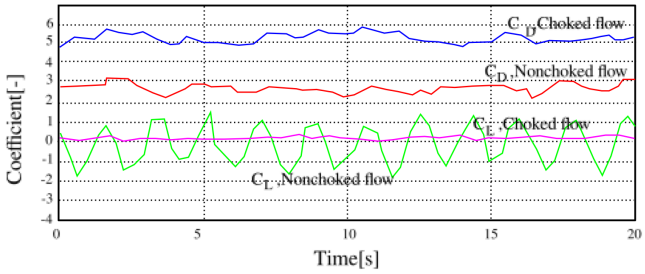

(a) Qi's experiment[6]

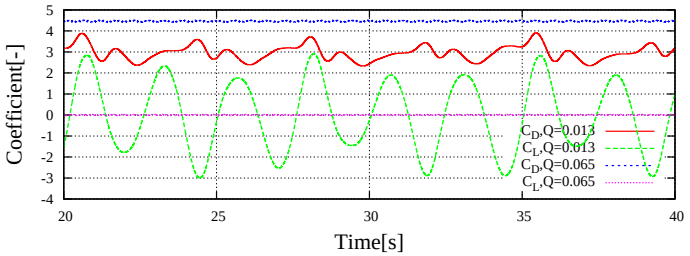

(b) Hydrostatic case

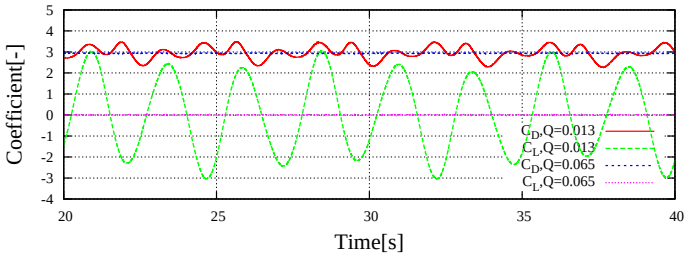

(c) 1 term non-hydrostatic case

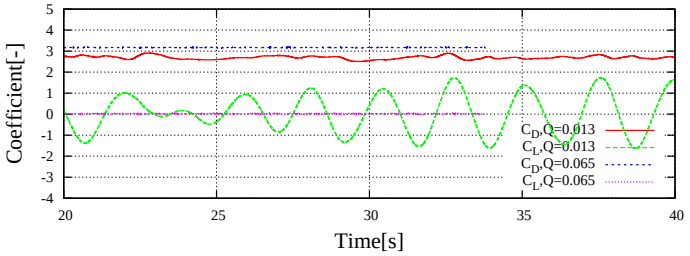

(d) 2 term non-hydrostatic case

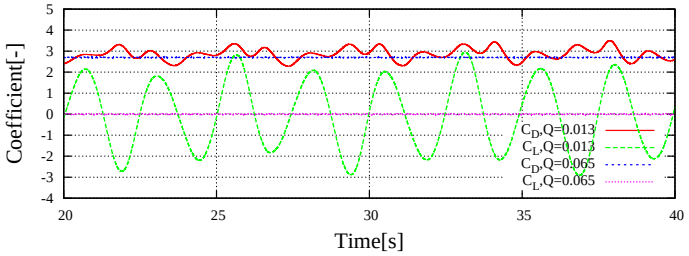

(e) Boussinesq non-hydrostatic case

Fig. 7 Time history of the drag and lift coefficients

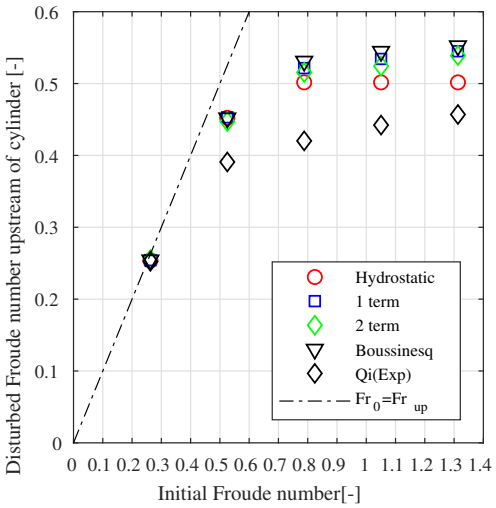

Fig. 8 Relationship between the initial Froude number and disturbed upstream Froude number

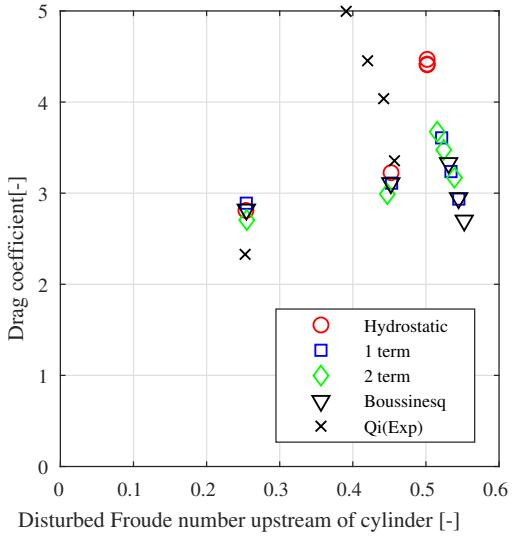

Fig. 9 Relationship between the disturbed upstream Froude number and drag coefficient

Table 2 Required computational time

Case	Computational time per required per time step	Max. possible time step for a fixed Courant No.	Required computational time to compute a given time interval
Hydrostatic	1	1	1
1 term,Boussinesq	2	2	1
2 term	5	2	2.5

Remark: Each column is normalized by the corresponding hydrostatic case value.

The relationship between the disturbed upstream Froude number and drag coefficient obtained from the simulations is shown in Fig.9 along with the experimental values of Qi. All non-hydrostatic cases are able to reproduce the trend observed in the experimental results, such that there exists a peak in the drag coefficient, but the disturbed upstream Froude number at which the peak is located is larger than the experiment and the peak value itself is smaller. The 2 term non-hydrostatic case has the largest peak value, followed by the 1 term case.

It should be noted that despite the fact that the 2 term NSWE solution is superior compared to the 1 term non-hydrostatic and hydrostatic SWEs, the time required to solve each time step is larger since one must solve more equations for more unknowns. The computational time required per time step, maximum possible time step for a fixed Courant No., and the required computational time to compute a given time interval is shown in Table 2, where each value is normalized by the corresponding hydrostatic SWE value. In the implementation in OpenFOAM employed for the simulations, the 2 term NSWE require approx. 2.5 times and the 1 term NSWE requires approx. 1 times the computational time required using the hydrostatic SWE to compute the solution for a given time interval.

5. Conclusions

In this paper, non-hydrostatic shallow water equations(NSWE) derived from the Navier-Stokes equation and continuity equation for incompressible fluids via the Galerkin method is presented. A linear profile with two degrees of freedom is assumed in the depth direction for the in-plane and depth direction velocities, and a quadratic profile with three degrees of freedom is assumed in the depth direction for the non-hydrostatic pressure. The interpolation functions for the velocities are defined to be orthogonal to each other, as are the linear and quadratic interpolation functions for the non-hydrostatic pressure, for better numerical conditioning. The presented approach results in 9 equations in 9 variables with a formulation which has structure and is strictly derived as a depth integrated equation.

Due to the addition of the non-hydrostatic components as well as the linearly varying velocities, the proposed equations have a theoretical linear dispersion relation that closely matches the exact linear dispersion relationship to a non dimensional wave number of approximately 10, and substantially better than the non-hydrostatic shallow water equations involving the Boussinesq assumption. The proposed NSWE are implemented into the opensource software OpenFOAM and the validity of the implementation is verified by comparing the numerical linear dispersion relationship with the theoretical relationship.

The applicability of the proposed NSWE in evaluating the lateral force applied to building structures is verified through comparison of simulated results with experimental results by Qi, in which the drag coefficient of square cylinders set in open channel flow are measured. The volume flux into the open channel is varied

with a constant initial water depth. As the volume flux is increased, the flow shifts from a non-choked state to a choked state, which the proposed NSWE are able to capture contrary to the hydrostatic shallow water equation. The fan like hydraulic jump for choked flows is properly reproduced as observed in the experiments, and the oscillatory behavior of the drag and lift coefficients are similar to the experiments. The relationship between the disturbed Froude number upstream of the cylinder and drag coefficient have the same feature as the experiment but with a smaller peak drag coefficient and larger corresponding Froude number. Despite the advantages of the proposed NSWE, it must be noted that since the formulation involves 9 equations in 9 variables, their solution requires approximately 2.5 times the time required for the hydrostatic formulation in computing the same time interval.

As future work, further investigation on the cause of the discrepancy of the drag coefficient with the experimental results will be conducted through detailed analysis and comparison with numerical simulations from a fully 3D CFD simulation.

6. Acknowledgements

This work was supported by JSPS KAKENHI Grant Number 18K04426(Grant-in-Aid for Scientific Research(C)).

7. References

[1] Castro-Orgaz, O., & Hager, W. (2017). Non-hydrostatic free surface flows. (Chap. 2). Springer International Publishing.

[2] Ghamry, H. K., & Steffler, P. M. (2002). Effect of applying different distribution shapes for velocities and pressure on simulation of curved open channels. *Journal of Hydraulic Engineering*, *128*(11), 969–982.

[3] Jeschke, A., Pedersen, G. K., Vater, S., & Behrens, J. (2017). Depth-averaged non-hydrostatic extension for shallow water equations with quadratic vertical pressure profile: Equivalence to boussinesq-type equations. *International Journal for Numerical Methods in Fluids*, *84*(10), 569–583.

[4] Liu, H., Li, M., & Shu, A. (2012). Large eddy simulation of turbulent shallow water flows using multi-relaxation-time lattice boltzmann model. *International Journal for Numerical Methods in Fluids*, *70*(12), 1573–1589.

[5] OpenFOAM The open source CFD toolbox. (n.d.). www.openfoam.com. Accessed: 2020-02-01.

[6] Qi, Z. X., Eames, I., & Johnson, E. R. (2014). Force acting on a square cylinder fixed in a free-surface channel flow. *Journal of Fluid Mechanics*, *756*, 716–727.

